NeuroImage 186 (2019) 146–154

Contents lists available at ScienceDirect

NeuroImage

journal homepage: www.elsevier.com/locate/neuroimage

Modular architecture of metabolic brain network and its effects on the spread of perturbation impact

Tianhao Zhang [a,b,1], Qi Huang [a,b,1], Chunxiang Jiao [e,f], Hua Liu [a,b], Binbin Nie [a,b], Shengxiang Liang [a,c], Panlong Li [a,c], Xi Sun [a,c], Ting Feng [a,c], Lin Xu [d,f,*], Baoci Shan [a,b,d,**]

[a] Beijing Engineering Research Center of Radiographic Techniques and Equipment, Institute of High Energy Physics, Chinese Academy of Sciences, Beijing, 100049, China
[b] School of Nuclear Science and Technology, University of Chinese Academy of Sciences, Beijing, 100049, China
[c] Department of Physics, Zhengzhou University, Zhengzhou, Henan, 450001, China
[d] CAS Center for Excellence in Brain Science and Intelligence Technology, Shanghai, China
[e] Yunnan Provincial Key Laboratory of Entomological Biopharmaceutical Research and Development, College of Pharmacy and Chemistry, Dali University, Dali, 671000, China
[f] Key Laboratory of Animal Models and Human Disease Mechanisms, and Laboratory of Learning and Memory, Kunming Institute of Zoology, Chinese Academy of Sciences, Kunming, 650223, China

ARTICLE INFO

Keywords:
FDG-PET
Metabolic connectivity
Brain network
Modularity
Perturbation

ABSTRACT

Metabolic brain network, which is based on functional correlation patterns of ^{18}F-fluorodeoxyglucose (FDG) positron emission tomography (PET) images, has been widely applied in both basic and clinical neuroscience. Exploring the properties of the metabolic brain network can provide valuable insight to the physiologic and pathologic processes of the brain. Based on the network theory, modular architecture has the ability to limit the spread of local perturbation impact and therefore modular networks are more robust against external damage. However, whether the metabolic brain network has modular architecture remains unknown.

Methods: 77 rats performed ^{18}F-FDG PET brain imaging. The metabolic brain network was then constructed by measuring interregional metabolic correlation in inter-subject manner. Afterwards, modular architecture of the network was detected by a greedy algorithm. Further, we perturbed the metabolic brain network by inducing focal photothrombotic ischemia in the bilateral motor cortex and then measured the glucose metabolic change of each brain region using FDG-PET.

Results: A significant modular architecture was found in the metabolic brain network. The network could be divided into four modules which corresponding approximately to executive, learning/memory, visual/auditory and sensorimotor processing functional domains. After inducing the focal ischemia on the bilateral motor cortex, most of the significantly changed brain regions (13 of 17) belong to the sensorimotor module.

Conclusion: Our results revealed an inherent modular architecture in the metabolic brain network and gave an experimental evidence that the modularity of the metabolism brain network could limit the spread of local perturbation impact.

1. Introduction

The brain is a complex system, which utilizes glucose as its main source of energy (Mergenthaler et al., 2013). Positron emission tomography (PET) with ^{18}F-Fluorodexyglucose (FDG) has been widely used to investigate brain glucose metabolism during physiologic and pathologic processes. In recent years, metabolic brain network based on FDG-PET images is emerging as a useful tool for both basic and clinical neuroscience (Yakushev et al., 2017), providing valuable insights into working memory (Zou et al., 2015), brain development (Choi et al., 2015) and

* Corresponding author. Kunming Institute of Zoology, Chinese Academy of Sciences, Kunming, 650223, China.
** Corresponding author. Institute of High Energy Physics, Chinese Academy of Sciences, Beijing, 100049, China.
E-mail addresses: thzhang@ihep.ac.cn (T. Zhang), huangq@ihep.ac.cn (Q. Huang), jiaocx_123@163.com (C. Jiao), liuhua@ihep.ac.cn (H. Liu), neibb@ihep.ac.cn (B. Nie), liangsx@ihep.ac.cn (S. Liang), lipl@ihep.ac.cn (P. Li), sunxi@ihep.ac.cn (X. Sun), fengt@ihep.ac.cn (T. Feng), lxu@vip.163.com (L. Xu), shanbc@ihep.ac.cn (B. Shan).
[1] Authors contributed equally to this work.

https://doi.org/10.1016/j.neuroimage.2018.11.003
Received 15 July 2018; Received in revised form 16 September 2018; Accepted 3 November 2018
Available online 5 November 2018
1053-8119/© 2018 Published by Elsevier Inc.

pathophysiology and diagnosis of many diseases such as epilepsy (Choi et al., 2014), Parkinson's disease (Huang et al., 2007; Tang et al., 2010), dementia with Lewy bodies (Caminiti et al., 2017) and Alzheimer's disease (Arnemann et al., 2018; Ballarini et al., 2016; Herholz et al., 2017; Morbelli et al., 2013; Perani et al., 2017).

Modularity, a network property that measured the tendency of nodes to cluster, has been revealed in various complex networks such as ecological networks (Olesen et al., 2007), cellular metabolism networks (Ravasz et al., 2002), and protein interaction networks (Han et al., 2004). In neuroscience, the modular architecture has also been discovered in the anatomical neural networks of elegans (Towlson et al., 2013) and the functional brain network of the human brain (He et al., 2009; Salvador et al., 2005; Schwarz et al., 2008). Moreover, further studies have revealed that each module of the human functional brain network often perform discrete cognitive function (Bertolero et al., 2015). Detecting modules can provide fundamental insights into the organization and function of the complex networks. However, the existence of modules in metabolic brain network is still largely unknown.

One advantage of modular architecture in the network is that it can limit the spread of local perturbations impact, and therefore the modular network is more resistant to external damage (Variano et al., 2004). This theoretical result has been recently verified in ecological networks (Gilarranz et al., 2017). Hence, if the metabolic brain network has a modular architecture, it is reasonable to hypothesize that the impact of focal damage would be largely limited to the module within which they originate. However, this hypothesize has remained untested.

In the present study, we constructed the metabolic brain network by 77 rats FDG-PET images and explored its modular architecture using a greedy algorithm. Then we perturbed the network by inducing a focal ischemia in the motor cortex and measured glucose metabolic change of each brain region after perturbation using FDG-PET. We hypothesized that (1) the metabolic brain network has a modular architecture; (2) the modularity of the network would limit the spread of local perturbation impact and therefore the impact of the motor cortex ischemia would be largely limited within the module to which motor cortex belonged.

2. Materials and Methods

2.1. Metabolic brain network construction and its modularity detection

2.1.1. Animals

77 adult male Sprague-Dawley rats (13–15 weeks old, weighing 280–320 g, Experimental Animal Center of the Academy of Military Medical Sciences, Beijing, China) were used for the metabolic brain network construction. All animals were kept in standard laboratory conditions (temperature at $23 \pm 2\,^{\circ}C$ and 12-h light/dark cycles) with free access to food and water. The rats were fasted for 12–15 h before ^{18}F-FDG injection. All animal experiments were performed with the approval of the Animal Care and Use Committee of the Chinese Academy of Sciences.

2.1.2. PET scanning

PET scanning was performed to get FDG-PET images. For each rat, ^{18}F-FDG (18.5 MBq/100 g of body weight) was injected via tail vein. Then the rats were kept in their home cages for 40 min. Then the rats were anesthetized with isoflurane (5% for induction and 2% for maintenance) and placed in a prone position on the scanning bed. The scanning was performed on a micro-PET system (E-plus 166, Institute of High Energy Physics, CAS, China) for 20 min. Afterwards, the images were reconstructed by Filtered Back projection algorithm and the reconstructed image matrix size was $128 \times 128 \times 63$ with the voxel size of $0.5 \times 0.5 \times 1\ mm^3$.

2.1.3. FDG-PET image preprocessing

All the 77 images were preprocessed using the spmratIHEP toolbox (Nie et al., 2014) based on SPM8 (Wellcome Department of Clinical Neurology, London, UK). First, the voxel size of all images was magnified 10 times in each dimension to approximate human brain size. Then, each image was spatially normalized to a standard FDG-PET rat brain template using the affine transformation and subsequent nonlinear warping. Finally, the partial volume effect was corrected by using PETPVE12 Toolbox (Gonzalez-Escamilla et al., 2017), and the intensity of the images was globally normalized.

2.1.4. Construction of metabolic brain networks

To generate the metabolic brain network, 48 anatomical brain regions (Table 1) were predefined by a 3D digital map based on the Paxinos & Watson atlas (Nie et al., 2013), and the average image intensity of each brain region of all subjects was extracted. Afterwards, the metabolic brain network was constructed by calculating Pearson correlation coefficient between each pair of brain regions in an inter-subject manner (Horwitz et al., 1984; Yakushev et al., 2017). The node of the network was represented by the brain region. The edge of the network was defined as the connection of each pair of nodes, and the weight of the edge was defined as the absolute value of correlation coefficients. The metabolic brain network was finally constructed as Fig. 1.

2.1.5. Modular architecture detection

The objective of the modular architecture detection algorithm is to find the partition that maximizes the modularity Q. The modularity Q is a scalar value that measures the density of links inside modules as compared to links between modules. In the case of weighted undirected network, the modularity Q is defined as (Newman, 2004):

$$Q = \frac{1}{2m}\sum_{i,j}[A_{ij} - \frac{k_i k_j}{2m}]\delta(m_i, m_j)$$

where A_{ij} represents the weight of the edge between node i and node j, k_i is the sum of weights attached to ties belonging to node i, m_i is the module to which node i is assigned, the Kronecker delta function $\delta(m_i, m_j)$ is 1 if $m_i = m_j$ (and 0 otherwise) and $m = \frac{1}{2}\sum_{ij} A_{ij}$.

Here, we adopted a greedy algorithm (Blondel et al., 2008) to maximize Q and detect the modular architecture of the metabolic brain

Table 1
Brain regions used for network construction.

Brain regions	Abbreviations	Paxinos Coordinates (mm)		
		x[a]	y	z
Anterior lobe of cerebellum	AL	1.98	4.74	−10.68
Amygdala	Amy	4.34	9.18	−3.24
Auditory cortex	Aud	6.99	4.62	−4.92
Cingulate gyrus	CG	0.86	1.73	1.08
Caudate putamen (striatum)	CPu	2.94	5.93	−0.12
Dentate gyrus	DG	3.56	5.34	−4.92
Entorhinal cortex	Ent	5.96	6.57	−7.08
Flocculonodular lobe	FL	5.13	6.63	−11.16
Frontal association cortex	FrA	1.69	3.12	5.77
Hippocampus	Hip	3.89	5.06	−5.40
Inferior colliculus	IC	2.03	4.35	−8.52
Insular cortex	INC	4.75	6.26	0.36
Motor cortex	Mot	2.23	1.69	2.28
Periaqueductal gray	PAG	0.78	5.60	−7.08
Prefrontal cortex	PFC	1.43	4.63	4.36
Posterior lobe of cerebellum	PL	2.77	5.04	−12.60
Posterior parietal cortex	PPC	5.71	2.39	−4.92
Parietal association cortex	ParA	3.15	1.49	−3.72
Retrosplenial cortex	RSC	1.31	2.07	−5.64
Superior colliculus	SC	1.60	4.53	−6.60
Sensory cortex	Sen	5.11	3.12	−0.60
Temporal association cortex	TeA	6.65	4.73	−7.08
Thalamus	Tha	2.11	6.15	−3.96
Visual cortex	Vis	3.97	1.82	−6.84

[a] We only showed the brain regions centroid coordinates in the right hemisphere since the brain has bilateral symmetry.

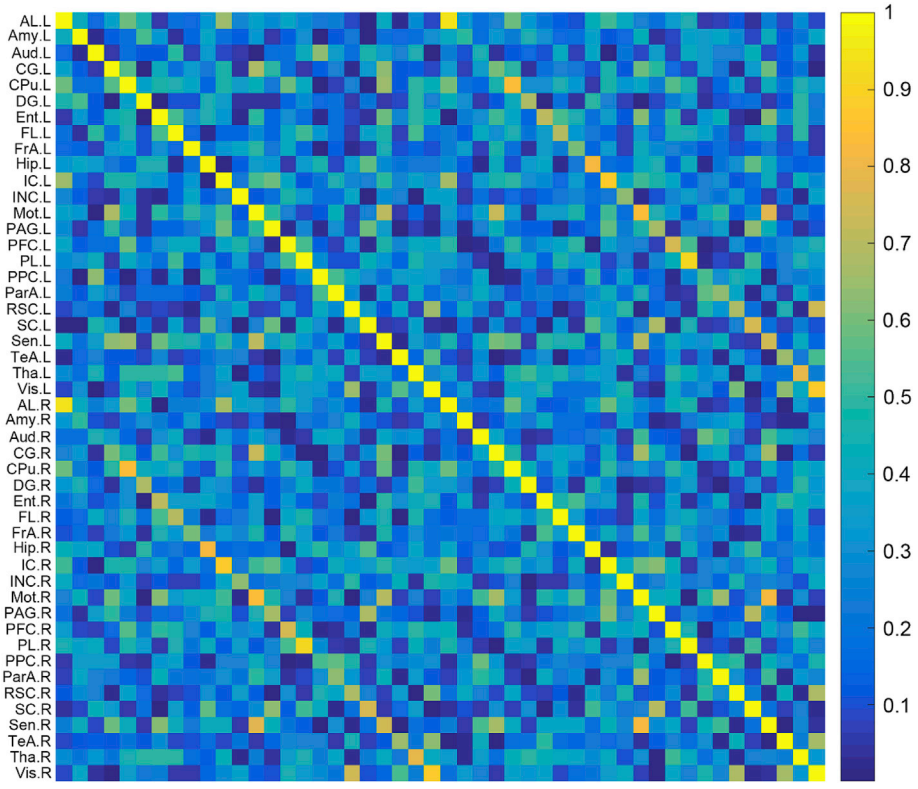

Fig. 1. Metabolic brain network acquired by calculating the absolute value of the Pearson correlation coefficient between each pair of brain regions.

network. In brief, the algorithm was divided into two iterative steps. At the first step, each node was treated as a different module. For each node i, it was moved into a module for which the increase of the Q is maximum and positive, and the process was repeated for all nodes. At the second step, a new weighted network was built. In the new network, the nodes were the modules found at the first phase. The weights of the edges between the new nodes were the sum of the weights of the edges between nodes in the corresponding two modules, and edges between nodes of the same module led to self-loops. Once the second step was completed, the first step of the algorithm was reapplied to the resulting weighted network and to iterate. The iteration was completed until no positive gain of Q.

The statistical significance of modularity of the metabolic brain network was evaluated by comparing it with 1000 comparable random networks. The random networks were generated by starting with a set of 48 unconnected nodes and randomly reorganizing the weighted-edges of the metabolic brain network between pairs of nodes. Then we used one-sample t-test to determine whether the modularity in the metabolic brain network was significantly different with that in random networks.

Once the optimized modular partition of the network was identified, we computed within-module degree z_i of each node (Guimera and Amaral, 2005). z_i measures how well-connected node i is to nodes in its own module, and z_i is defined as:

$$z_i = \frac{\kappa_i - \overline{\kappa}_{m_i}}{\sigma_{\kappa_{m_i}}}$$

where $\kappa_i = \sum_{j \neq i} A_{ij}\delta(m_i, m_j)$ is the sum of the weight between node i and other nodes in its module m_i. $\overline{\kappa}_{m_i}$ is the average of κ over all the nodes in m_i, and $\sigma_{\kappa_{m_i}}$ is the standard deviation of κ in m_i. A node was defined as hub node if $z_i > 1$. The hub nodes have stronger connections to other nodes within its own module than non-hub nodes, thus the hub nodes might play important roles in information integration and communication within modules (van den Heuvel and Sporns, 2013). Therefore, computing hub nodes of each module can help us to identify the function of each module in brain.

2.2. Modular metabolic brain network perturbation

To test whether the modular architecture of the metabolic brain network could limit the spread of the local perturbation impact, we induced focal photothrombotic ischemia in the bilateral motor cortex to mimic the local perturbation, and then measured the metabolic change of each brain region.

Photothrombotic model is a quick, minimally-invasive technique for inducing small and well-delimited ischemia in a highly reproducible manner (Labat-gest & Tomasi, 2013). Ten rats (nine for FDG-PET scanning and one for histological analysis) were used to establish the photothrombotic ischemia model. Seven rats were performed sham-operation and then underwent FDG-PET scanning. These 17 rats had the same age range, body weight range and feeding conditions as for the 77 rats described before.

2.2.1. Photothrombotic ischemia model

Photothrombotic ischemia was induced according to a previously published protocol (Diederich et al., 2014). A schematic was shown in Fig. 2. In brief, under deep anesthesia with Sodium pentobarbital (8 mg/100 g of body weight, intraperitoneal injection), rats were infused with Rose Bengal (4 mg/100 g of body weight, Sigma-Aldrich) via tail vein. After 10 min, a laser beam was stereotaxically positioned at a distance of 1 mm from the skull on the bilateral hemisphere ($x = \pm 2.0$mm and $z = 2.0$mm in Paxions space) through an optic fiber (1 mm interior diameter), using two diode-pumped solid-state DPSS crystal lasers (CL-2000; Reno, NV 89502, U.S.A) working at 473 nm. The skull was irradiated for 20 min. Body temperature was kept at 37 °C using a thermoregulated pad during experiments. Sham-operated animals underwent the same procedure including Bengal Rose injection but without illumination. All rats survived from brain ischemia.

After modeling 24 h, one rat was TTC (2,3,5-triphenyltetrazolium

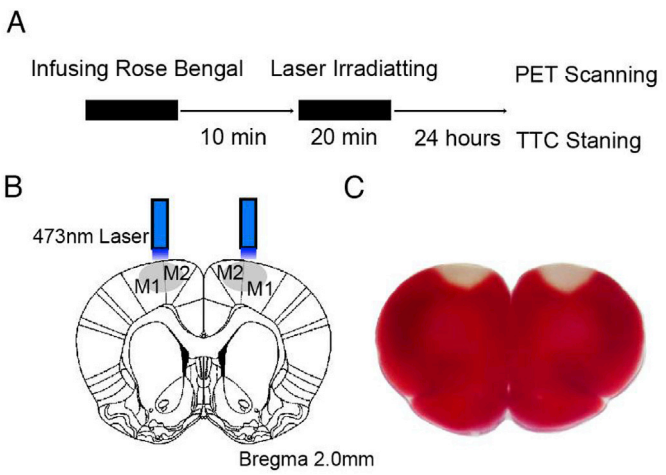

Fig. 2. A schematic for inducing photothrombotic ischemia. (A) A flowchart for modeling. (B) The modeling location showed on the coronal plane of rat brain atlas. (C) TTC staining for showing photothrombosis-induced focal ischemia in 24 h after modeling.

chloride) stained to show the ischemic area (Fig. 2C). The rat was anesthetized and perfused with saline buffer and 4% paraformaldehyde dissolved in phosphate buffer saline. The brain was removed from the cranium and incubated for 30 min at 37 °C in 1% TTC solution. Brain sections (400 μm) obtained by vibratome (Leica VT1000) were immediately immersed into 1% TTC solution at 37 °C for 15 min.

2.2.2. Metabolic change of each brain region after local perturbation

After establishing the photothrombotic model, the rats were kept in their home cages for 24 h, then PET scanning was performed. PET scanning and image preprocessing were consistent with the previous description. Nine rats which performed photothrombotic ischemia were assigned to the model group and seven sham-operated rats were assigned to the control group. To detect the significantly metabolic changed regions after bilateral motor cortex lesions, we extracted mean intensity of the 48 brain regions of each rat. Two-sample *t*-test was then performed between model and control group on all brain regions, and the significant level was set at $P < 0.05$ (two-tailed).

To quantitatively test whether nodes in different modules respond to the local perturbation differently, the *t* value from two-sample *t*-test of a given region was regarded as the magnitude of the metabolic change for this region, and Kruskal-Wallis *H* test followed by Dunn's test for post hoc analysis was performed on the *t* values. The Kruskal-Wallis *H* test (Kruskal and Wallis, 1952) is a non-parametric version of classical one-way analysis of variance (ANOVA) for testing whether three or more independent groups differ. In this study, the nodes in different modules were regarded as different groups. The null hypothesis of the Kruskal-Wallis test is that the medians of groups are all equal. Therefore, a significant test statistics ($H < 0.05$) indicates that at least the median of one group is different from the median of at least one other group. After Kruskal-Wallis test, Dunn's test (Dunn, 1964), a post hoc non parametric test, was used to do multiple pairwise comparisons between groups and to find out which pairs of them are significant. Dunn's test calculates a P value for each pair of groups. A value of $P < 0.05$ was considered statistically significant. All statistical analyses were performed using IBM SPSS Statistics 23.

Further, to test the hypothesis that the modular architecture of the metabolism brain network could limit the spread of local perturbation impact, a permutation test was performed. We regarded the number of the brain regions whose metabolism was significantly changed in other modules (modules except the module that contains motor cortex) as the test statistic. Then we randomly reassigned the brain regions into different modules 10^6 times without changing the number of modules (four modules, see Results 3.1), number of modules' regions (8,8,14,18 respectively, see Results 3.1) and the magnitude of the metabolic change of each region. If the observed number of the significantly changed regions in other modules (4 of 17, see Results 3.2) is significantly less than that in the random cases, we considered the hypothesis is acceptable.

3. Results

3.1. Modular architecture of rat metabolic brain network

We constructed the metabolic brain network using 77 awake rat brain FDG-PET images and then detected its modular architecture. The maximum modularity ($Q = 0.16$) was reached when the network was separated into 4 modules (Fig. 3A–B) and significant modularity ($P < 0.001$) was found in the network (Fig. 3B–C). Therefore, the metabolic brain network could be divided into four modules based on the maximum modularity without any prior knowledge of regional functions.

Four modules and the hub nodes of each module were shown in Fig. 4. Module I (red) comprised four pairs of bilateral brain regions, including the prefrontal cortex, posterior lobe of cerebellum, flocculonodular lobe and thalamus. The hub nodes of module I were the left posterior lobe of cerebellum. Module II (green) comprised four pairs of the bilateral brain regions which were the hippocampus, dentate gyrus, amygdala and superior colliculus. The hub nodes of module II were the bilateral hippocampus. Module III (blue) comprised seven pairs of bilateral brain regions which were the visual cortex, auditory cortex, retrosplenial cortex, temporal association cortex, parietal association cortex, posterior parietal cortex and insular cortex. The hub nodes of module III were the right visual cortex and bilateral retrosplenial cortex. Module IV (yellow) comprised nine pairs of bilateral brain regions including the motor cortex, sensory cortex, anterior lobe of cerebellum, cingulate gyrus, inferior colliculus, entorhinal cortex, striatum, frontal association cortex and periaqueductal gray. The hub nodes were the bilateral motor cortex and left sensory cortex.

3.2. Metabolic change after local perturbation

We perturbed the metabolic brain network by inducing focal ischemia in the bilateral motor cortex (Fig. 2) and then measured the glucose metabolic change of each brain region (Fig. 5A). We found that the glucose metabolism of 17 brain regions (13 brain regions belonged to module IV, 2 brain regions belonged to module II and 2 brain regions belonged to module III) was significantly ($P < 0.05$, two-tailed) changed after ischemia (Fig. 5B). Force-directed graph layout (Fruchterman and Reingold, 1991) of the metabolic brain network also provided an intuitive way to visualize the impact of perturbation on modular network in a topological space, and visualizations were provided at a threshold which used the least edges that preserved full connectedness (Fig. 5C).

To quantitatively test whether the brain regions in the different modules respond to the local perturbation differently (see Materials and Methods 2.2.2), we performed Kruskal-Wallis *H* test followed by Dunn's test for post hoc analysis. Kruskal-Wallis *H* test showed that the impact of local perturbation on the bilateral motor cortex among four modules was significantly different ($H = 0.004$). Then, Dunn's test found that module IV was significantly different with module I ($P = 0.001$) and module III ($P = 0.010$), and the comparisons of the rest four pairs were not significantly different (module I vs. module II: $P = 0.056$; module I vs. module III: $P = 0.284$; module II vs. module III: $P = 0.278$; module II vs. module IV: $P = 0.299$). Together with the result that most of the significantly changed brain regions (13 of 17) belonged to the module IV (Fig. 5C), these results indicated that different modules respond to the local perturbation on the bilateral motor cortex differently and module IV was the most affected module.

Further, to test whether the modular architecture of the metabolic brain network would limit the spread of the local perturbation, we performed a permutation test. If the modular architecture could limit the

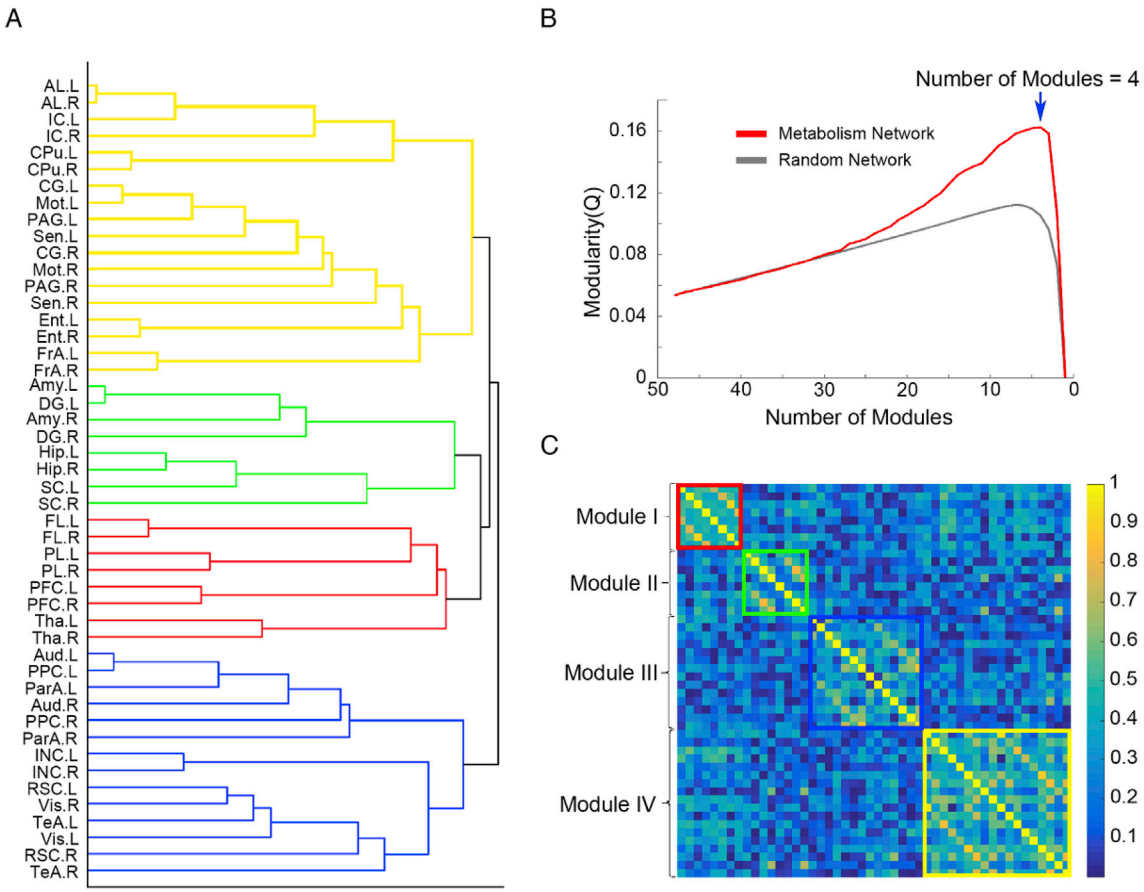

Fig. 3. Identification of the modular architecture in the metabolic brain network. (A) Dendrogram of the modules identification progress determined by modularity *Q*. (B) Progress of the network modularity *Q* for the metabolic brain network (red line) and mean *Q* of 1000 matched random networks (gray line) as regions were merged into modules. The maximum modularity ($Q = 0.16$) was reached when the metabolic brain network was separated into 4 modules, indicated by the blue arrow. (C) Correlation matrix whose nodes were ordered by module assignments. The color bar indicates the connection strength.

impact of perturbation, the number of the significantly changed regions outside module IV (4 of 17) would be significantly less than that in the random cases. Indeed, after 10^6 times random reassignment of the module labels to the brain regions, the mean and standard deviation number of significantly changed regions outside module IV is 10.63 ± 1.62, and that the cases that the number of significantly changed regions outside the module IV was less than or equal to four only occurred 54 times, so the P value was estimated as $54/10^6 = 5.4 \times 10^{-5}$. Therefore, these statistical results supported that the modular architecture of metabolic brain network could limit the spread of the local perturbation.

4. Discussion

In the present study, we first constructed a metabolic brain network using 77 rat brain FDG-PET images and detected the modular architecture of the metabolic brain network by using a greedy algorithm. The network was divided into four modules, and the brain regions as well as the hub nodes of each module were then identified. These results demonstrated an intrinsically cohesive modular architecture in the metabolic brain network. Further, we measured metabolic changes of each brain region after perturbing the network by inducing focal ischemia in the bilateral motor cortex, and found that the brain regions with significant metabolic change were mostly located in the module to which motor cortex belonged. These findings provided an evidence that the modular architecture of the network could limit the spread of external perturbations.

Modularity is a general hallmark of complex biological systems (Sporns and Betzel, 2016). The highly modularized architecture of brain metabolic brain network elucidated in this study represents a general organizational principle of metabolic brain networks, which is consistent with the concept that modularity is a key property of brain networks (Sporns and Betzel, 2016). Modularity in brain networks have also been revealed by other neuroimaging techniques such as functional magnetic resonance imaging (fMRI) (He et al., 2009; Salvador et al., 2005), structural magnetic resonance imaging (Chen et al., 2008), diffusion spectrum imaging (Hagmann et al., 2008), and EEG studies (Liu et al., 2014). These studies using different techniques consistently demonstrated that the brain functional and anatomical networks have modular architectures.

Detecting modules in the brain networks can uncover major building blocks, which are often corresponding to functional components (Bertolero et al., 2015). The hub nodes have stronger connections in their own modules than non-hub nodes. Therefore, the hub nodes might be crucial to maintain the communication within the modules (van den Heuvel and Sporns, 2013), thus, their function might partly determine the main function of their module. In this study, we detected four modules in the metabolic brain network, and identified the hub nodes of each module. The hub node of module I was left posterior lobe of cerebellum. Although the cerebellum's role in motor function is well recognized, cumulative evidences from studies of neuroanatomy, neuroimaging and neuropsychology has indicated the cerebellum plays an important role in executive function (Koziol et al., 2014; Sokolov et al., 2017; Stoodley and Schmahmann, 2009; Strick et al., 2009). Other brain regions in module I are also known to be associated with executive functions (Dalley et al., 2004; Haber and Calzavara, 2009). The hub nodes of module II were the

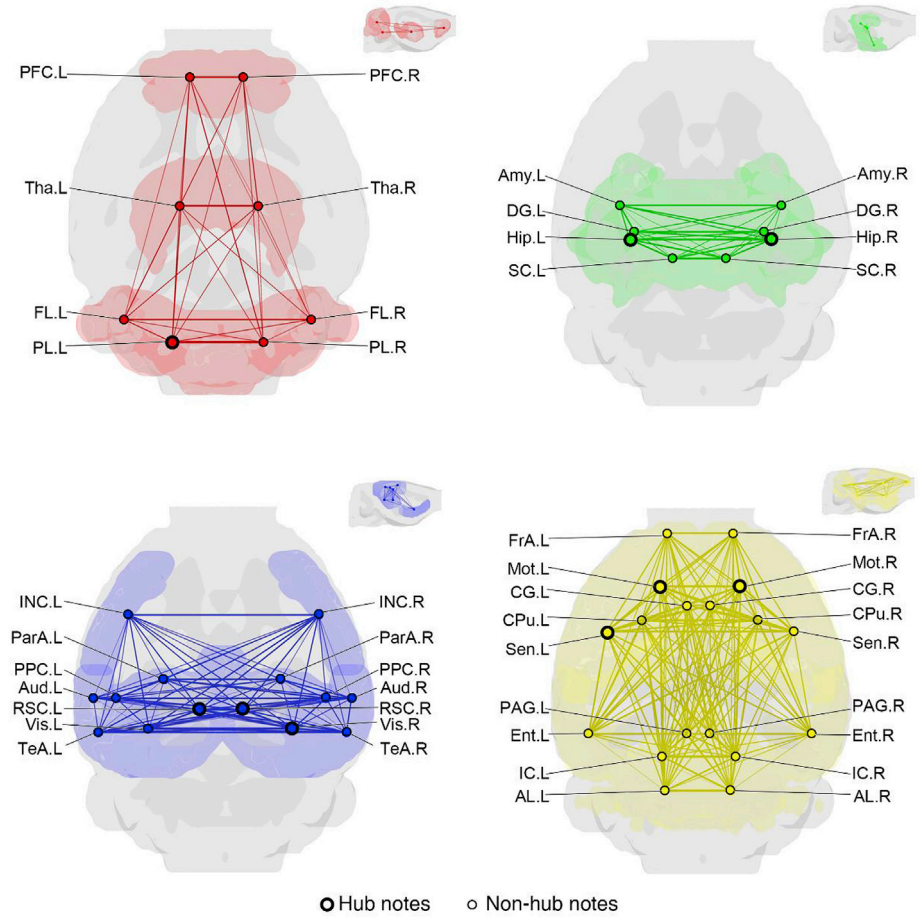

Fig. 4. Four modules and the brain regions of each module. Module I, II, III, IV were presented in the upper left, upper right, lower left and lower right of the figure respectively. The hub nodes and non-hub nodes of each module are marked by black annulus.

bilateral hippocampus. The hippocampus and other regions in module II such as amygdala and dentate gyrus are primarily involved in learning and memory (Bliss and Collingridge, 1993; Cahill et al., 1995), which indicates that the main function of module II is learning and memory. The hub nodes of module III were the right visual cortex and bilateral retrosplenial cortex. Visual cortex is the central region for processing visual information. A recent study also showed that the retrosplenial cortex could receive and process both sound and scene information from auditory cortex and visual cortex respectively (Li et al., 2018). Other brain regions in module III are also associated with visual and auditory processing (Bamiou et al., 2003; Kravitz et al., 2011; Shomstein and Yantis, 2006). Therefore, the main function of module III is likely to be visual and auditory processing. The hub nodes in module IV were the bilateral motor cortex and left sensory cortex, which are well known to be crucial for sensorimotor processing (Penfield and Boldrey, 1937; Sanes and Donoghue, 2000). Some other brain regions in module IV, such as striatum and anterior lobe of cerebellum, are also the critical components of the sensorimotor systems (Heimer et al., 1982; Schmahmann, 2007). Thus the primary function of module IV might be sensorimotor processing. Taken together, the metabolic brain network could be divided into four modules, which mainly associated with executive, learning/-memory, visual/auditory and sensorimotor processing.

The brain needs to be robust to adapt to a changing environment. Meanwhile, brains are physically expensive systems and they need high metabolic costs to maintain the normal physiological processes (Bullmore and Sporns, 2012). Therefore, the architecture of the metabolic brain network is likely to reflect a trade-off between increasing robustness and minimizing wiring costs. The modular architecture itself might contribute to the adaptability and robustness of the brain system (Kashtan and Alon, 2005; Kashtan et al., 2007). Meanwhile, our results showed that each module closely overlapped with known functional domains. These results might reflect an evolutionary drive to place functionally related brain regions into the same module, therefore reducing the total cost of wiring. Moreover, a simulation study showed the modular networks were much more efficient than non-modular networks if connective density must be kept low to reduce energy needs (Tosh and McNally, 2015).

A benefit of modular organization is increased robustness in response to sudden perturbations. In the present study, the network was perturbed by inducing focal ischemia in the bilateral motor cortex, and only 4 of 17 brain regions were significantly changed outside modules IV, which was less than that in most of the random cases. This result suggests that the modular metabolic brain network could buffer the spread of local perturbation impact, and is consistent with prior studies that the modular architecture could increase the robustness and flexibility of the system (Kashtan and Alon, 2005). However, the glucose metabolism of some regions in module IV were not significantly changed, which might indicate that although modular architecture can limit the spread of local perturbation, not all regions in the module would be significantly affected. This result might explain why the Dunn's test between module IV and module II are not statistical significant. Meanwhile, most extremely changed brain regions after perturbation were located in the sensorimotor module (module IV). This result supports the concept derived from recent studies evaluating the effect of local perturbation on functional brain networks that the brain regions which functionally connect with perturbed regions could be more easily affected than other regions (Chan et al., 2017; Grayson et al., 2016). The damage of a brain region mainly caused alteration of brain regions in the damaged module,

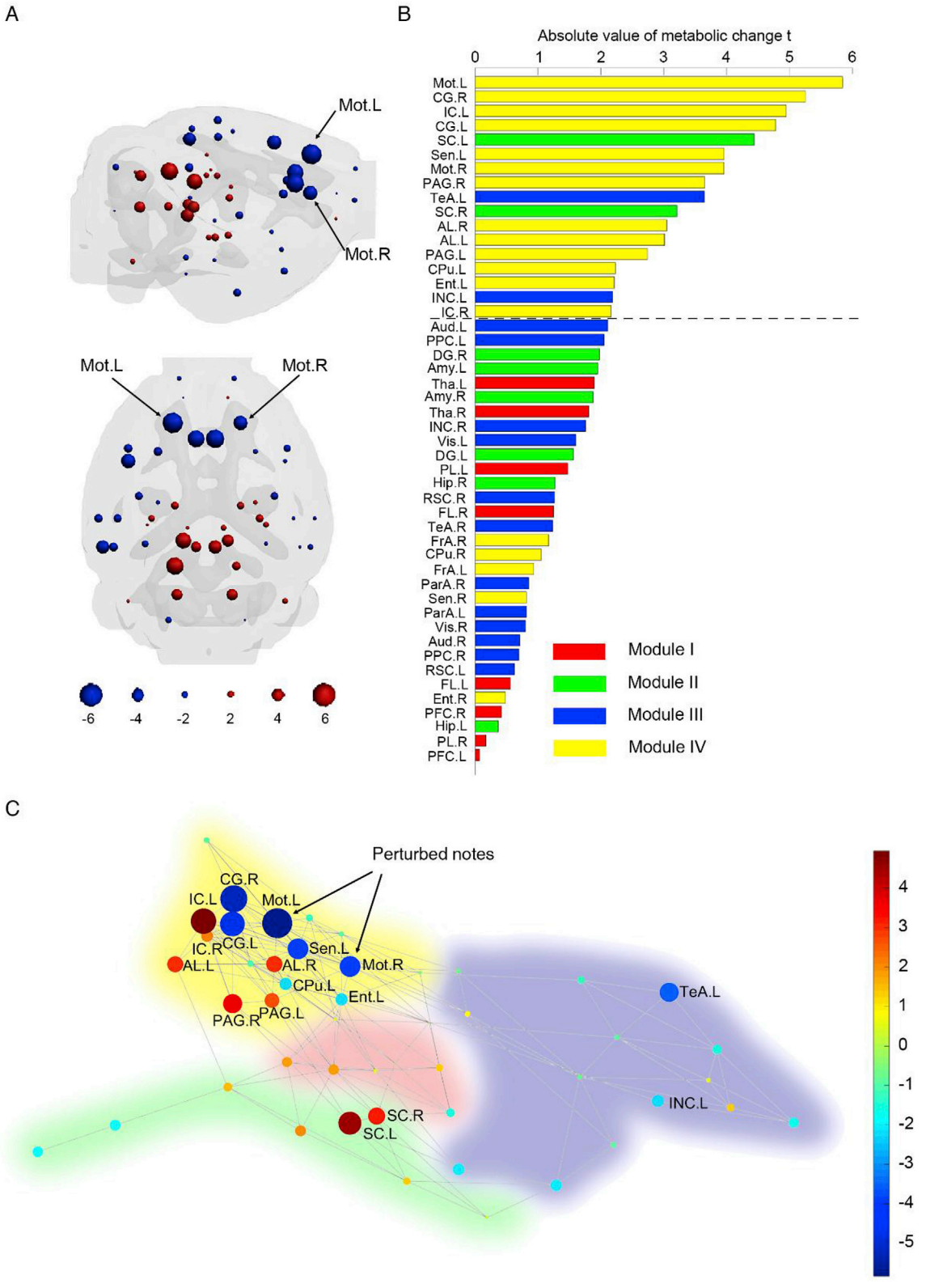

Fig. 5. Metabolic change of each region after motor cortex ischemia. (A) Metabolic changes showed in anatomical space. Blue balls represented hypometabolism and red balls represented hypermetabolism. The size of the balls denoted the magnitude of the metabolic changes. (B) Absolute *t* value of each brain region sorted high to low. The metabolisms of 17 brain regions were significant different (two-tailed, $P < 0.05$) between control and model groups (above dotted line). Each region was color-coded according to its module. (C) The metabolic changes showed in topological space. The background colors of red, green, blue and yellow represented module I, II, III, IV respectively. The color and size of nodes both denoted the magnitude of the metabolic change. The color bar indicates the metabolic change of each region. Only 17 significant different regions were marked.

suggesting the autonomy of modules' functions (Bertolero et al., 2015). Moreover, several studies of patients with focal brain lesions have demonstrated that the effect of focal damage extends beyond the lesion area (Gratton et al., 2012; Nomura et al., 2010). Our results implied that the local brain lesions may have widely impact on the brain regions within the same module, which may explain some of nonspecific functional deficits in diseases with local pathologies such as brain tumor or stroke.

To ensure that proximity to the perturbed regions was not a determining factor to the results, we computed the distance between perturbed regions (bilateral motor cortex) and other brain regions. The distance of a brain region to bilateral motor cortex was defined as the average distance of the region to left motor cortex and right motor cortex. The statistical difference of the mean distances of the affected regions and unaffected regions was tested. Although the mean distance (8.37 ± 4.02 mm) of affected regions to perturbed regions were slightly shorter than that of unaffected regions (9.21 ± 3.16 mm), the result was not statistically significant ($P = 0.473$, two-tailed *t*-test). Therefore, we speculated that the spatial distance to the perturbation regions might slightly affect the results but might not be a determining factor.

In this study, we gave an experimental evidence that the modularity of the metabolism brain network could hinder the global spreading. However, it should be noticed that some brain regions which have high connection strength to the perturbation regions were barely affected (such as right sensory cortex and right parietal association cortex), and some brain regions which have weak connection to the perturbation regions were significantly affected (such as left temporal association cortex and left superior colliculus). These uncoupling between the magnitude of impacts and the connection strength to the perturbation regions might reflect the complexity of perturbation impact spreading in the complex network. Many factors such as the location of the perturbation site, the interaction of different subnetworks and the global topology of the network might affect the spread of the impact (Misic et al., 2015; Nematzadeh et al., 2014). Therefore, the relationship between the magnitude of impacts and the strength of the connections to the perturbed regions might be non-linear. In the future, more precise and subtle models of spreading dynamics should be developed to describe and predict the spread of the perturbation impact in the metabolic brain network.

Several methodological considerations need to be stated about this study. First, most studies of modularity of brain networks removed negative edge weights from the analysis because very few modular detection algorithms are capable of dealing with negative edge weight (Sporns and Betzel, 2016). Similarly, we defined the edge weights of the network as the absolute value of correlation coefficients instead of correlation coefficients themselves, It should be noted that this step might unintentionally discard neurobiological information. Second, since the problem of modularity optimization is non-deterministic polynomial-time hard (NP-hard) (Brandes et al., 2008), numerous maximize modularity algorithms have been developed and different algorithms may yield different results. In this study, we adopt a widely used algorithm developed by Blondel et al. (2008). The accuracy of the algorithm was verified on ad hoc modular networks that had a known community structure in their article. Third, in this study, we perturbed the network by inducing focal ischemia on bilateral motor cortex to test the hypothesis that the modular architecture could limit the spread of local perturbation. However, many other factors, such as the perturbation method or the magnitude of the perturbation, may affect the spread of the impact and thereby possibly affect the outcomes. Furthermore, the location of the perturbed regions may be also crucial to the results (Gratton et al., 2012). Therefore, further investigations are needed to examine the hypothesis more thoroughly by, e.g., using a variety of perturbation methods and regulating various additional brain regions. In future applications, it will be important to investigate how the modularity of the metabolic brain network change in the animal models with focal brain damage such as stoke, traumatic brain injury or brain tumors.

5. Conclusion

In this study, we constructed a metabolic brain network and explored its modular architecture. Significant modular architecture was found in the metabolic brain network, and the network could be divided into four modules, which closely overlapped with executive, learning/memory, visual/auditory and sensorimotor processing functional domains. Then we perturbed the network by inducing focal ischemia on bilateral motor cortex and measured the glucose metabolic changes of all brain regions. We found that most of the significantly changed brain regions were located in the sensorimotor module. Together, these results revealed an intrinsically cohesive modular architecture in the metabolic brain network, and provided an experimental evidence that the modular architecture can limit the spread of local perturbation impact.

Disclosure

The authors have no conflicts of interest to disclose.

Acknowledgments

We would like to thank Dr. Kewei Chen for constructive criticism of the manuscript.

This work was supported by the National Natural Science Foundation of China [grant numbers 81471741, 81471728, 81671770].

References

Arnemann, K.L., et al., 2018. Metabolic brain networks in aging and preclinical Alzheimer's disease. Neuroimag-Clin 17, 987–999. https://doi.org/10.1016/j.nicl.2017.12.037.

Ballarini, T., et al., 2016. Neuropsychiatric subsyndromes and brain metabolic network dysfunctions in early onset Alzheimer's disease. Hum. Brain Mapp. 37 (12), 4234–4247. https://doi.org/10.1002/hbm.23305.

Bamiou, D.E., et al., 2003. The insula (Island of Reil) and its role in auditory processing literature review. Brain Res. Rev. 42 (2), 143–154. https://doi.org/10.1016/s0165-0173(03)00172-3.

Bertolero, M.A., et al., 2015. The modular and integrative functional architecture of the human brain. Proc. Natl. Acad. Sci. U. S. A 112 (49), E6798–E6807. https://doi.org/10.1073/pnas.1510619112.

Bliss, T.V.P., Collingridge, G.L., 1993. A Synaptic model of memory - long-term potentiation in the hippocampus. Nature 361 (6407), 31–39. https://doi.org/10.1038/361031a0.

Blondel, V.D., et al., 2008. Fast unfolding of communities in large networks. J. Stat. Mech. Theor. Exp. https://doi.org/10.1088/1742-5468/2008/10/p10008.

Brandes, U., et al., 2008. On modularity clustering. IEEE Trans. Knowl. Data Eng. 20 (2), 172–188. https://doi.org/10.1109/tkde.2007.190689.

Bullmore, E.T., Sporns, O., 2012. The economy of brain network organization. Nat. Rev. Neurosci. 13 (5), 336–349. https://doi.org/10.1038/nrn3214.

Cahill, L., et al., 1995. The amygdala and emotional memory. Nature 377 (6547), 295–296. https://doi.org/10.1038/377295a0.

Caminiti, S.P., et al., 2017. Metabolic connectomics targeting brain pathology in dementia with Lewy bodies. J. Cerebr. Blood Flow Metabol. 37 (4), 1311–1325. https://doi.org/10.1177/0271678x16654497.

Chan, R.W., et al., 2017. Low-frequency hippocampal-cortical activity drives brain-wide resting-state functional MRI connectivity. Proc. Natl. Acad. Sci. U. S. A 114 (33), E6972–E6981. https://doi.org/10.1073/pnas.1703309114.

Chen, Z.J., et al., 2008. Revealing modular architecture of human brain structural networks by using cortical thickness from MRI. Cerebr. Cortex 18 (10), 2374–2381. https://doi.org/10.1093/cercor/bhn003.

Choi, H., et al., 2015. Maturation of metabolic connectivity of the adolescent rat brain. Elife 4. https://doi.org/10.7554/eLife.11571.001.

Choi, H., et al., 2014. Abnormal metabolic connectivity in the pilocarpine-induced epilepsy rat model: a multiscale network analysis based on persistent homology. Neuroimage 99, 226–236. https://doi.org/10.1016/j.neuroimage.2014.05.039.

Dalley, J.W., et al., 2004. Prefrontal executive and cognitive functions in rodents: neural and neurochemical substrates. Neurosci. Biobehav. Rev. 28 (7), 771–784. https://doi.org/10.1016/j.neubiorev.2004.09.006.

Diederich, K., et al., 2014. Cortical photothrombotic infarcts impair the recall of previously acquired memories but spare the formation of new ones. Stroke 45 (2), 614–618. https://doi.org/10.1161/strokeaha.113.001907.

Dunn, O.J., 1964. Multiple comparisons using rank sums. Technometrics 6 (3), 241–&. https://doi.org/10.2307/1266041.

Fruchterman, T.M.J., Reingold, E.M., 1991. Graph drawing by force-directed placement. Software Pract. Ex. 21 (11), 1129–1164. https://doi.org/10.1002/spe.4380211102.

Gilarranz, L.J., et al., 2017. Effects of network modularity on the spread of perturbation impact in experimental metapopulations. Science 357 (6347), 199–201. https://doi.org/10.1126/science.aal4122.
Gonzalez-Escamilla, G., et al., 2017. PETPVE12: an SPM toolbox for Partial Volume Effects correction in brain PET Application to amyloid imaging with AV45-PET. Neuroimage 147, 669–677. https://doi.org/10.1016/j.neuroimage.2016.12.077.
Gratton, C., et al., 2012. Focal brain lesions to critical locations cause widespread disruption of the modular organization of the brain. J. Cognit. Neurosci. 24 (6), 1275–1285. https://doi.org/10.1162/jocn_a_00222.
Grayson, D.S., et al., 2016. The rhesus monkey connectome predicts disrupted functional networks resulting from pharmacogenetic inactivation of the amygdala. Neuron 91 (2), 453–466. https://doi.org/10.1016/j.neuron.2016.06.005.
Guimera, R., Amaral, L.A.N., 2005. Cartography of complex networks: modules and universal roles. J. Stat. Mech. Theor. Exp. https://doi.org/10.1088/1742-5468/2005/02/p02001.
Haber, S.N., Calzavara, R., 2009. The cortico-basal ganglia integrative network: the role of the thalamus. Brain Res. Bull. 78 (2–3), 69–74. https://doi.org/10.1016/j.brainresbull.2008.09.013.
Hagmann, P., et al., 2008. Mapping the structural core of human cerebral cortex. PLoS Biol. 6 (7), 1479–1493. https://doi.org/10.1371/journal.pbio.0060159.
Han, J.D.J., et al., 2004. Evidence for dynamically organized modularity in the yeast protein-protein interaction network. Nature 430 (6995), 88–93. https://doi.org/10.1038/nature02555.
He, Y., et al., 2009. Uncovering intrinsic modular organization of spontaneous brain activity in humans. PLoS One 4 (4). https://doi.org/10.1371/journal.pone.0005226.
Heimer, L., et al., 1982. Ventral striatum and ventral pallidum - components of the motor system. Trends Neurosci. 5 (3), 83–87. https://doi.org/10.1016/0166-2236(82)90037-6.
Herholz, K., et al., 2017. Metabolic regional and network changes in Alzheimer's disease subtypes. J. Cerebr. Blood Flow Metabol. https://doi.org/10.1177/0271678X17718436, 271678X17718436.
Horwitz, B., et al., 1984. Intercorrelations of glucose metabolic rates between brain-regions - application to healthy-males in a state of reduced sensory input. J. Cerebr. Blood Flow Metabol. 4 (4), 484–499. https://doi.org/10.1038/jcbfm.1984.73.
Huang, C.R., et al., 2007. Metabolic brain networks associated with cognitive function in Parkinson's disease. Neuroimage 34 (2), 714–723. https://doi.org/10.1016/j.neuroimage.2006.09.003.
Kashtan, N., Alon, U., 2005. Spontaneous evolution of modularity and network motifs. Proc. Natl. Acad. Sci. U. S. A 102 (39), 13773–13778. https://doi.org/10.1073/pnas.0503610102.
Kashtan, N., et al., 2007. Varying environments can speed up evolution. Proc. Natl. Acad. Sci. U. S. A 104 (34), 13711–13716. https://doi.org/10.1073/pnas.0611630104.
Koziol, L.F., et al., 2014. Consensus paper: the cerebellum's role in movement and cognition. Cerebellum 13 (1), 151–177. https://doi.org/10.1007/s12311-013-0511-x.
Kravitz, D.J., et al., 2011. A new neural framework for visuospatial processing. Nat. Rev. Neurosci. 12 (4), 217–230. https://doi.org/10.1038/nrn3008.
Kruskal, W.H., Wallis, W.A., 1952. Use of ranks in one-criterion variance analysis. J. Am. Stat. Assoc. 47 (260), 583–621.
Labat-gest, V., Tomasi, S., 2013. Photothrombotic ischemia: a minimally invasive and reproducible photochemical cortical lesion model for mouse stroke studies. Jove-J. Vis. Exp. 76 https://doi.org/10.3791/50370.
Li, P., et al., 2018. Structural and functional brain network of human retrosplenial cortex. Neurosci. Lett. 674, 24–29. https://doi.org/10.1016/j.neulet.2018.03.016.
Liu, Y., et al., 2014. Network community structure detection for directional neural networks inferred from multichannel multisubject EEG data. IEEE Trans. Biomed. Eng. 61 (7), 1919–1930. https://doi.org/10.1109/tbme.2013.2296778.
Mergenthaler, P., et al., 2013. Sugar for the brain: the role of glucose in physiological and pathological brain function. Trends Neurosci. 36 (10), 587–597. https://doi.org/10.1016/j.tins.2013.07.001.
Misic, B., et al., 2015. Cooperative and competitive spreading dynamics on the human connectome. Neuron 86 (6), 1518–1529. https://doi.org/10.1016/j.neuron.2015.05.035.
Morbelli, S., et al., 2013. Metabolic networks underlying cognitive reserve in prodromal Alzheimer disease: a european Alzheimer disease consortium project. J. Nucl. Med. 54 (6), 894–902. https://doi.org/10.2967/jnumed.112.113928.
Nematzadeh, A., et al., 2014. Optimal network modularity for information diffusion. Phys. Rev. Lett. 113 (8) https://doi.org/10.1103/PhysRevLett.113.088701.
Newman, M.E.J., 2004. Analysis of weighted networks. Phys. Rev. 70 (5) https://doi.org/10.1103/PhysRevE.70.056131.
Nie, B.B., et al., 2013. A rat brain MRI template with digital stereotaxic atlas of fine anatomical delineations in paxinos space and its automated application in voxel-wise analysis. Hum. Brain Mapp. 34 (6), 1306–1318. https://doi.org/10.1002/hbm.21511.
Nie, B.B., et al., 2014. A statistical parametric mapping toolbox used for voxel-wise analysis of FDG-PET images of rat brain. PLoS One 9 (9). https://doi.org/10.1371/journal.pone.0108295.
Nomura, E.M., et al., 2010. Double dissociation of two cognitive control networks in patients with focal brain lesions. Proc. Natl. Acad. Sci. U. S. A 107 (26), 12017–12022. https://doi.org/10.1073/pnas.1002431107.
Olesen, J.M., et al., 2007. The modularity of pollination networks. Proc. Natl. Acad. Sci. U. S. A 104 (50), 19891–19896. https://doi.org/10.1073/pnas.0706375104.
Penfield, W., Boldrey, E., 1937. Somatic motor and sensory representation in the cerebral cortex of man as studied by electrical stimulation. Brain 60, 389–443. https://doi.org/10.1093/brain/60.4.389.
Perani, D., et al., 2017. The impact of bilingualism on brain reserve and metabolic connectivity in Alzheimer's dementia. Proc. Natl. Acad. Sci. U. S. A 114 (7), 1690–1695. https://doi.org/10.1073/pnas.1610909114.
Ravasz, E., et al., 2002. Hierarchical organization of modularity in metabolic networks. Science 297 (5586), 1551–1555. https://doi.org/10.1126/science.1073374.
Salvador, R., et al., 2005. Neurophysiological architecture of functional magnetic resonance images of human brain. Cerebr. Cortex 15 (9), 1332–1342. https://doi.org/10.1093/cercor/bhi016.
Sanes, J.N., Donoghue, J.P., 2000. Plasticity and primary motor cortex. Annu. Rev. Neurosci. 23, 393–415. https://doi.org/10.1146/annurev.neuro.23.1.393.
Schmahmann, J., 2007. The primary motor cerebellum is in the anterior lobe but not the posterior lobe. evidence from stroke patients. Neurology 68 (12). A357-A357.
Schwarz, A.J., et al., 2008. Community structure and modularity in networks of correlated brain activity. Magn. Reson. Imag. 26 (7), 914–920. https://doi.org/10.1016/j.mri.2008.01.048.
Shomstein, S., Yantis, S., 2006. Parietal cortex mediates voluntary control of spatial and nonspatial auditory attention. J. Neurosci. 26 (2), 435–439. https://doi.org/10.1523/jneurosci.4408-05.2006.
Sokolov, A.A., et al., 2017. The cerebellum: adaptive prediction for movement and cognition. Trends Cognit. Sci. 21 (5), 313–332. https://doi.org/10.1016/j.tics.2017.02.005.
Sporns, O., Betzel, R.F., 2016. Modular brain networks. In: Fiske, S.T. (Ed.), Annual Review of Psychology, vol. 67, pp. 613–640, 67.
Stoodley, C.J., Schmahmann, J.D., 2009. Functional topography in the human cerebellum: a meta-analysis of neuroimaging studies. Neuroimage 44 (2), 489–501. https://doi.org/10.1016/j.neuroimage.2008.08.039.
Strick, P.L., et al., 2009. Cerebellum and nonmotor function. Annu. Rev. Neurosci. 32, 413–434. https://doi.org/10.1146/annurev.neuro.31.060407.125606.
Tang, C.C., et al., 2010. Abnormalities in metabolic network activity precede the onset of motor symptoms in Parkinson's disease. J. Neurosci. 30 (3), 1049–1056. https://doi.org/10.1523/jneurosci.4188-09.2010.
Tosh, C.R., McNally, L., 2015. The relative efficiency of modular and non-modular networks of different size. Proc. R. Soc. Lond. B Biol. Sci. 282 (1802) https://doi.org/10.1098/rspb.2014.2568.
Towlson, E.K., et al., 2013. The rich club of the C. elegans neuronal connectome. J. Neurosci. 33 (15), 6380–6387. https://doi.org/10.1523/jneurosci.3784-12.2013.
van den Heuvel, M.P., Sporns, O., 2013. Network hubs in the human brain. Trends Cognit. Sci. 17 (12), 683–696. https://doi.org/10.1016/j.tics.2013.09.012.
Variano, E.A., et al., 2004. Networks, dynamics, and modularity. Phys. Rev. Lett. 92 (18) https://doi.org/10.1103/PhysRevLett.92.188701.
Yakushev, I., et al., 2017. Metabolic connectivity: methods and applications. Curr. Opin. Neurol. 30 (6), 677–685. https://doi.org/10.1097/wco.0000000000000494.
Zou, N., et al., 2015. Metabolic connectivity as index of verbal working memory. J. Cerebr. Blood Flow Metabol. 35 (7), 1122–1126. https://doi.org/10.1038/jcbfm.2015.40.